Structure and Solvation of Mercury(II) Iodide, Bromide, and Chloride in Pyridine Solution; Refinement of the Crystal Structure of Di-iodobis(pyridine)mercury(II), $[HgI_2(py)_2]$†

Ingmar Persson
Inorganic Chemistry 1, Chemical Center, University of Lund, P.O. Box 124, S-221 00 Lund, Sweden
Magnus Sandström*
Department of Inorganic Chemistry, The Royal Institute of Technology, S-100 44 Stockholm, Sweden
Peter L. Goggin
Department of Inorganic Chemistry, The University, Bristol BS8 1TS
Alain Mosset
Laboratoire de Chimie de Coordination du C.N.R.S., B.P. 4142-31030, Toulouse Cedex, France

The structure of the neutral mercury(II) halides in pyridine (py) solution has been studied by *X*-ray diffraction methods and vibrational spectroscopy. Pseudo-tetrahedral $HgX_2(py)_2$ species (X = I, Br, or Cl) are formed in solution with approximately C_{2v} symmetry. Relevant bond lengths are Hg–I 2.665(2), Hg–Br 2.497(2), and Hg–Cl 2.375(10) Å. The IHgI angle was found to be 143(2)° and BrHgBr 151(3)°, including estimated corrections for shrinkage effects. The two pyridine molecules have Hg–N distances of 2.43(2), 2.45(2), and 2.47(2) Å in the iodide, bromide, and chloride species, respectively. The crystal structure of $[HgI_2(py)_2]$ has been refined to an *R* value of 0.031 for 744 observations. It consists of monomeric pseudo-tetrahedral $[HgI_2(py)_2]$ species with Hg–I bond lengths of 2.664(1) and 2.668(1) Å and an IHgI angle of 142.7(1)°. The two pyridine ligands are related by a mirror plane which contains the HgI_2 entity. The Hg–N distance is 2.424(9) Å. Raman and i.r. spectra of the pyridine solutions and of the $HgX_2(py)_2$ solids are consistent with structural models based on the diffraction data.

The solid-state structures of the bis(pyridine) complexes of mercury(II) halides have been studied extensively by spectroscopic and diffraction methods.[1,2] The compounds $[HgBr_2(py)_2]$ and $[HgI_2(py)_2]$ consist of discrete molecular complexes with four-co-ordinated mercury and XHgX angles of 141 and 143°, respectively. The $HgCl_2(py)_2$ structure is of a different type and comprises six-co-ordinated mercury in doubly chloride-bridged square-planar $(HgCl_2)_n$ chains with the pyridine ligands in *trans*-octahedral positions.[2] However, in pyridine solution mercury(II) seems to form complexes of the same type for all three halides. For dilute solutions (< 16 mmol dm^{-3} Hg^{II}) only mononuclear complexes with from one to four halides on mercury have been found in the course of equilibrium and enthalpy measurements.[3] According to these measurements at least 97% of the mercury complexes present in pyridine solutions of HgX_2 are neutral with increasing stability in the order X = Cl < Br < I.

In order to correlate the co-ordinating properties of the solvent with the change in structure of the solvated HgX_2 molecules, combined *X*-ray diffraction and Raman and i.r. spectroscopic studies of concentrated solutions of HgX_2 in donor solvents have been undertaken.[4] The present paper concerns an extension of these studies to pyridine as solvent. To provide a basis for models of the molecular complexes in solution, crystal structure determinations of the solvates $HgX_2(py)_2$ were initiated. After completion of the work for X = Cl and I, structure determinations for all three solvates were reported.[2] Our results for $HgCl_2(py)_2$ are in agreement within the estimated standard deviations given; however, we obtained much better quality single crystals of $[HgI_2(py)_2]$ and, consequently, now report our more precise parameters.

† *Supplementary data available* (No. SUP 56235, 3 pp.): thermal parameters. See Instructions for Authors, *J. Chem. Soc., Dalton Trans.*, 1985, Issue 1, pp. xvii–xix. Structure factors are available from the editorial office.

Table 1. Composition of the investigated solutions. The linear absorption coefficient μ is given for Mo-K_α radiation, and the density ρ was measured at 25 °C

	X		
	I	Br	Cl
$[HgX_2]$/mol dm^{-3}	0.700	0.725	0.901$_5$
$[C_5H_5N]$/mol dm^{-3}	11.70	11.85	11.80
μ/cm^{-1}	23.7	26.9	22.5
ρ/g cm^{-3}	1.243	1.199	1.180

Experimental

Preparation of Samples.—Weighed amounts of recrystallized and vacuum-dried mercury(II) halides were dissolved in pyridine (Merck p.a.). The solvent had been dried by treatment with 3-Å molecular sieves. Pale yellow crystals of $[HgI_2(py)_2]$ were obtained by slow cooling of a saturated solution.

The compositions of the solutions investigated are given in Table 1.

Solution X-Ray Diffractometry.—A large-angle theta–theta diffractometer, previously described,[5] was used to measure the *X*-ray scattering (Mo-K_α radiation, λ = 0.7107 Å) from the surface of pyridine solutions at 25 ± 1 °C. During the main part of the data collection the solutions were enclosed inside a thin-walled (0.15 mm) half-filled cylindrical glass vessel of about 30 mm in diameter. This was positioned with its axis horizontal and perpendicular to the *X*-ray beam. The absorption in the glass walls was measured by comparing the intensities from a 3 mol dm^{-3} aqueous solution of $Na_2[HgI_4]$ in this cylinder with those determined using an open cup. The intensity ratio varied smoothly from 0.65 to 0.56:1 in the accessible range θ = 5—70° (the meniscus inside the glass cylinder prevented measurements

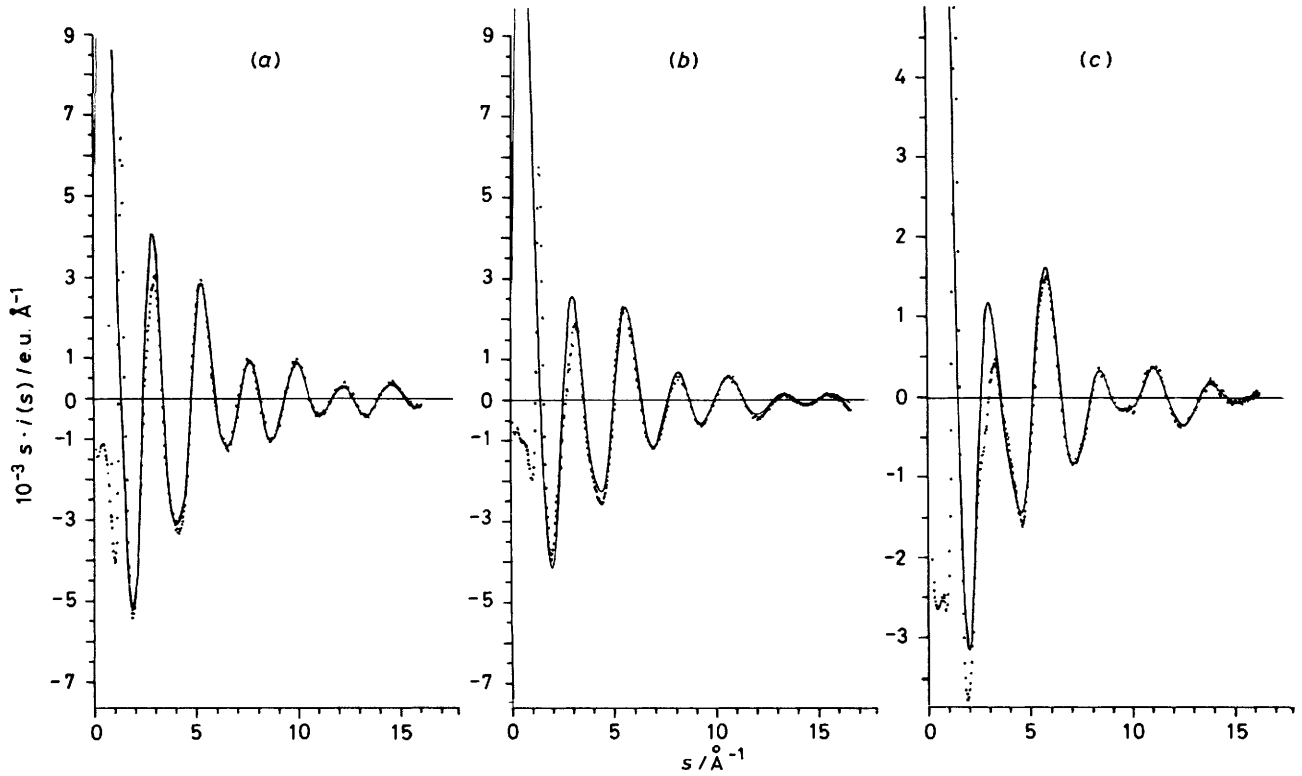

Figure 1. Experimental (dots) and calculated (solid lines) $si(s)$ values of HgI_2 (*a*), $HgBr_2$ (*b*), and $HgCl_2$ (*c*) in pyridine. Parameters given in Table 5 for the molecular $HgX_2(py)_2$ species were used for the theoretical curves

at lower angles), and this was used to correct the experimental intensities.

The scattering was sampled twice at discrete points at intervals of 0.1° for $5 < \theta < 20°$ and of 0.25° for $\theta > 20°$ (the diffraction angle is 2θ). At least 100 000 counts were accumulated at each point, corresponding to a statistical error of about 0.3%. For the region $1 < \theta < 5°$ scans of 10 000 counts were made at 0.1° intervals for solutions in filled, open glass cups contained in an outer cylinder with a Mylar window to minimize evaporation. The divergence angle of the primary *X*-ray beam was limited by 1, $\frac{1}{4}$, or $\frac{1}{12}$° slits, with overlap between the sets of measurements for the purposes of scaling.

All calculations were carried out using the KURVLR and PUTSLR computer programs.[6] The same data-reduction procedures as described previously were applied.[5,7] The experimental intensities were normalized to a stoicheiometric unit of volume, *V*, corresponding to one mercury atom. The reduced-intensity curves, $i(s)$, multiplied by the scattering variable $s = (4\pi/\lambda)\sin\theta$, are shown in Figure 1.

By a Fourier transformation, the differential radial distribution functions (r.d.f.s) were obtained from equation (1)

$$D(r) - 4\pi r^2\rho_0 = (2r/\pi)\int_0^{s_{max.}} si(s)\cdot M(s)\sin(rs)\mathrm{d}s \quad (1)$$

where r is the interatomic distance in real space and $\rho_0 = \{[\sum_i f_i(0)]^2 + [\sum_i \Delta f_i'']^2\}/V$. The neutral atom scattering factor $f(s)$ was corrected for the real part $\Delta f'$ of the anomalous dispersion of which $\Delta f''$ is the imaginary part.[8] All summations are taken over all atoms in the stoicheiometric unit of volume. The modification function chosen was as in equation (2). Its effect is appreciably to sharpen the peaks in the r.d.f.s [solid lines in Figure 2(*a*)], but its exponential damping part only moderately reduces the sinusoidal variations of the $si(s)$ integral kernel at the finite cut-off limit at $s_{max.} = 16$ Å^{-1}. Therefore, damped oscillations occur around the sharpest peaks due to the truncation effects of the Fourier integral. In the present study, the analysis of the scattering data has been based mainly on the comparison of calculated peak shapes with experimental r.d.f.s. The highest possible resolution is therefore needed. The calculated model intensity functions (3), where r_{pq} is the distance

$$M(s) = \mathrm{e}^{-0.01s^2}\left[\sum_i f_i(0)\right]^2 \Big/ \left[\sum_i f_i(s)\right]^2 \quad (2)$$

$$i_c(s) = \sum_{p\neq q}\sum_q \left\{f_p(s)f_q(s) + \Delta f_p''\Delta f_q''\right\}\sin(sr_{pq})(sr_{pq})^{-1}\exp(-l_{pq}^2s^2/2) \quad (3)$$

between the atoms p and q and l^2 its mean-square variation, are modified and transformed in the same way as the experimental $i(s)$ curves.[6] Thus, the peak shapes so obtained (Figure 2) will be affected by the same type of distortions as the peaks in the r.d.f. and in a difference function these effects will cancel. The chosen $M(s)$ function was therefore considered to be adequate for this type of data analysis.

Crystallography for $[HgI_2(py)_2]$.—*Crystal data.* $C_{10}H_{10}HgI_2N_2$, $M = 612.7$, orthorhombic, space group *Pnma* (no. 62), $a = 14.564(4)$, $b = 11.395(2)$, $c = 8.528(2)$ Å, $U = 1\,415.4(6)$ Å^3, $Z = 4$, $D_c = 2.87$ g cm^{-3}, $F(000) = 1\,080$, $\mu = 153$ cm^{-1} (Mo-K_α), specimen size 0.18 × 0.18 × 0.16 mm enclosed in a capillary.

A Syntex $P2_1$ automatic four-circle diffractometer was used

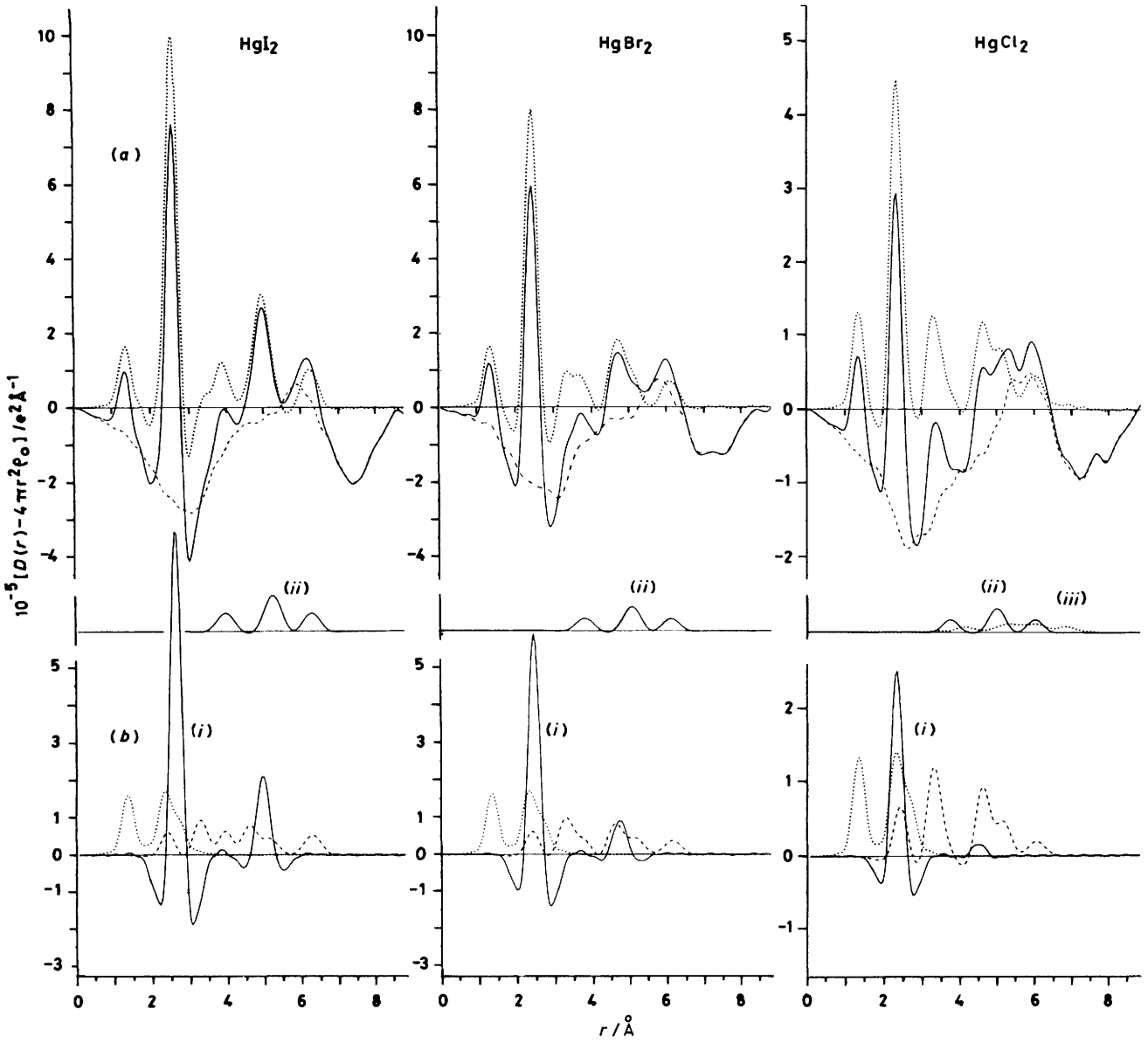

Figure 2. $D(r) - 4\pi r^2\rho_0$ functions and calculated peak shapes with parameters from Table 5. (*a*) Experimental curves (solid lines), model functions (dotted lines), and their differences (dashed curve); (*b*) model functions separated into the intramolecular pyridine peak shapes (dotted lines), Hg–X and X • • • X peak shapes [solid lines (*i*)], Hg–py and those X • • • py interactions which do not vary during rotation of the pyridine ligands (dashed lines), variable X • • • C distances [solid lines (*ii*)], and for the $HgCl_2(py)_2$ model estimated py • • • py interactions between the two ligands [dashed line (*iii*)]

to sample a unique data set consisting of 979 independent *hkl* reflections for $2\theta < 45°$ in ω-scan mode. The intensities of 744 reflections were greater than $3\sigma(I)$ and were used in the calculations. The unit-cell parameters were determined by a least-squares refinement on 25 selected reflections centred on the diffractometer. A semiempirical absorption correction was applied.[9] The SHELX 76 program system was used with full-matrix least-squares refinements.[10] Neutral atom scattering factors with anomalous dispersion corrections were used.[8]

In the final cycles of refinement anisotropic thermal parameters were kept only for the Hg and I atoms, as the introduction of anisotropy for the N and C atoms did not significantly improve the weighted agreement factor R'. Hydrogen atoms were included with positional parameters at calculated trigonal values (C–H 1.08 Å) and a common thermal parameter refined to $U_H = 0.09(2)$ Å^2. Final agreement factors were $R = 0.031$ and $R' = 0.035$ with reflection weights set at $1/[\sigma^2(F_o) + 0.0025F_o^2]$. An isotropic extinction parameter was refined to $x = 7.6(6) \times 10^{-8}$ where $F_c = F(1 - xF^2\sin\theta)$. The largest shift in the parameters was 0.06σ. The ten highest remaining ripples (between 0.9 and 0.5 e Å^{-3}) in a Fourier difference map based on the final parameters were all located around the heavy atoms.

The refined atomic co-ordinates are given in Table 2, and the mercury environment is compared with that of $[HgBr_2(py)_2]$ in Table 3.[2] The same unit-cell orientation and atomic numbering as in ref. 2 have been used. A picture of the $[HgI_2(py)_2]$ molecule is shown in Figure 3.

Vibrational Spectra.—Infrared spectra were measured with a Nicolet 7199A Fourier-transform spectrometer using a 6.25-μm Mylar beam splitter (range 500—100 cm^{-1}), Globar source, and

Table 2. Non-hydrogen atom parameters with estimated standard deviations in parentheses for $[HgI_2(py)_2]$

Atom	*x*	*y*	*z*
Hg	0.004 45(4)	$\frac{1}{4}$	0.066 07(7)
I(A)	0.164 4(1)	$\frac{1}{4}$	0.218 4(1)
I(B)	−0.068 7(1)	$\frac{1}{4}$	−0.220 2(1)
N	−0.079 7(5)	0.405 2(8)	0.196 8(11)
C(2)	−0.130 9(7)	0.482 9(9)	0.117 6(14)
C(3)	−0.180 3(7)	0.569 2(11)	0.190 9(15)
C(4)	−0.178 1(8)	0.575 7(12)	0.348 5(16)
C(5)	−0.123 8(8)	0.499 3(10)	0.436 9(14)
C(6)	−0.074 0(7)	0.417 4(11)	0.353 0(15)

Table 3. Intramolecular mercury environment (distances in Å, angles in °) in the crystal structures of $[HgI_2(py)_2]$ and $[HgBr_2(py)_2]$

	$[HgI_2(py)_2]$	$[HgBr_2(py)_2]$[a]
Hg–X(A)	2.668(1)	2.478(3)
Hg–X(B)	2.664(1)	2.483(3)
Hg–N	2.424(9)	2.38(2), 2.39(2)
X(A)–Hg–X(B)	142.7(1)	141.2(1)
X(A)–Hg–N	102.6(2)	102.5(5), 103.9(5)
X(B)–Hg–N	102.7(2)	103.2(5), 104.3(4)
N–Hg–N^{i}[b]	93.8(4)	90.7(7)

[a] From ref. 2, Table 5. [b] Symmetry code: i $x, \frac{1}{2}-y, z$ for $[HgI_2(py)_2]$.

DTGS detector with polyethylene windows. Solutions in pyridine were examined using cells with high-density polyethylene windows (pathlength 0.5 mm). For comparison, measurements were also made of solutions in dimethyl sulphoxide (dmso) and methanol; for the methanol solutions and $HgCl_2$ in dmso a pathlength of 0.015 mm between silicon windows was used.

Solids were finely ground and dispersed in Nujol to which a small amount of pyridine had been added; spectra were recorded without delay since the samples lose pyridine after some time.

Raman spectra were excited with a Coherent Radiation Laboratories Innova 90-5 argon-ion laser using the 514.5-nm line. Spectra were recorded with a D.I.L.O.R. RTI 30 triple monochromator using d.c. amplification, normally with a spectral bandwidth of 4 cm^{-1} for the solutions and 1 cm^{-1} for the solids.

Results

Crystal Structure of $[HgI_2(py)_2]$.—A general description of the structure has been given in ref. 2 and mainly features of special interest as regards the molecular structure in solution will be discussed here. The unit cell contains four discrete $[HgI_2(py)_2]$ molecules with Hg and I atoms located on a crystallographic mirror plane (Figure 3 in ref. 2). The mercury atom co-ordinates two I and two N atoms in a pairwise symmetrical pseudo-tetrahedral arrangement with the I(A),Hg,I(B) and N,Hg,N^{i} planes almost perpendicular (Figure 3). The only significant deviation from an internal *mm* point symmetry (C_{2v}) is that the pyridine ligands are twisted by 27.7° around the Hg–N bond, *i.e.* the angle between the normals to the N,Hg,N^{i} plane and the pyridine-ring plane, which contains the Hg atom, is 117.7°.

The molecular geometry is very similar to that found in the crystal structure of $[HgBr_2(py)_2]$, although the compounds are not isostructural.[2] Table 3 shows that the XHgX and NHgN angles are 1.5(1) and 3.1(8)°, respectively, smaller in the bromide compound and the Hg–N bond length seems to be slightly shorter. In the bromide the twist angles of the pyridine rings around the Hg–N bonds are smaller, 2.4 and 16.4°, than in the iodide compound. This means that the $[HgBr_2(py)_2]$ molecule is closer to an internal C_{2v} symmetry than is $[HgI_2(py)_2]$, despite its lack of crystallographic point-symmetry elements.

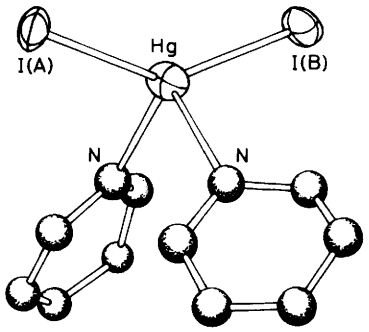

Figure 3. The $[HgI_2(py)_2]$ molecule. The Hg and I atoms are represented by 30% probability ellipsoids. The carbon atoms are numbered sequentially around the ring starting with C(2)

Vibrational Spectra.—The symmetric and asymmetric stretching frequencies (Table 4) of the XHgX entities in pyridine solution show good agreement with previously reported Raman studies.[11] The vibrational spectra of the solid $HgX_2(py)_2$ compounds have been investigated previously.[1] It was concluded that the bromide and iodide complexes have monomeric tetrahedral structures. The wavenumbers obtained (Table 4 and ref. 1) agree well with the solution values, and it is evident that the XHgX geometry is similar. However, in solution $HgCl_2$ clearly has a structure different from that of solid $HgCl_2(py)_2$, where all Cl atoms are bridging.[2] The wavenumbers obtained are typical of terminal Hg–Cl stretches of $HgCl_2$ in a co-ordinating solvent.[11] As pointed out previously,[4,11] the occurrence of asymmetrical stretching frequencies in the Raman spectra demonstrates that the HgX_2 entity is non-linear. Thus, it seems very probable that all three HgX_2 complexes in pyridine solution have similar geometries.

The interpretation of the solution i.r. spectra was facilitated by interactive subtraction of a spectrum of pure pyridine to remove unperturbed solvent features. Broad bands could then be discerned in the bromide and iodide solutions which approximately corresponded to $Hg(py)_2$ vibrations in the solid compounds. The values obtained support the suggestion from the *X*-ray diffraction studies that the Hg–N bonds in $[HgBr_2(py)_2]$ and $[HgI_2(py)_2]$ are of similar type in the solid and in solution.

An attempt was also made to look for minor species in the $HgCl_2$ solution by subtraction of solvent-corrected spectra for a 0.1 mol dm^{-3} solution from a 0.9 mol dm^{-3} solution with appropriate factors to eliminate the stretching frequencies at about 300 cm^{-1}. Three low-frequency peaks appeared at about 250, 200, and 168 cm^{-1}. The interpretation of these is not clear, but if they are real, they are probably connected with observation from the *X*-ray diffraction results that a slight dissociation (*ca.* 5%) of the $HgCl_2$ molecules seems to have occurred.

Solution X-Ray Data.—The radial distribution functions, r.d.f. = $D(r) - 4\pi r^2\rho_0$ [solid lines in Figure 2(*a*)], show distinct major peaks at 2.7, 2.5, and 2.4 Å for the HgI_2, $HgBr_2$, and $HgCl_2$ solutions, respectively. The mean Hg–X distances, 2.67

Table 4. Vibrational frequencies (cm^{-1}) for the HgX_2 solutions in pyridine and for $HgX_2(py)_2$ crystalline solvates (s = strong, m = medium, w = weak, v = very, sh = shoulder, br = broad, p = polarized). The assignments given are mainly based on the arguments in ref. 1

	Solution		Crystalline $HgX_2(py)_2$			
	I.r.	Raman	I.r. *ca.* 300 K	Raman *ca.* 300 K	Raman *ca.* 100 K	Assignment
HgI_2	181s	180w	176s	173w	175w	$\nu_{asym}(HgI_2)$
	ca. 138w,br	142s,p	145m	139s	145s, 143w (sh), 140w	$\nu_{sym}(HgI_2)$
			140w (sh)		155w, 151w, 137w	$\nu_{sym}[Hg(py)_2]$
	ca. 125w,br		125s	121m (sh)	129m, 126w	$\nu_{asym}[Hg(py)_2]$
$HgBr_2$	222.5s	222w	217s	216w	222vw (sh), 218w	$\nu_{asym}(HgBr_2)$
	184.8m	183s,p	182m	182s	183s	$\nu_{sym}(HgBr_2)$
	ca. 136w,br		141w	143w	158m, 148w, 136vw, 130vw	$\nu_{sym}[Hg(py)_2]$
	112w,br		114m	112w	115m, 100w	$\nu_{asym}[Hg(py)_2]$
$HgCl_2$	313s	313w				$\nu_{asym}(HgCl_2)$
	287m (sh)	282s,p				$\nu_{sym}(HgCl_2)$
	ca. 250w					$\nu_{asym}(HgCl_3^-)$
	ca. 200w,br					$\nu[Hg(py)_6^{2+}]$
	ca. 168w					
			ca. 160m,br			*
			123s,br			*
			ca. 93m,br			*

* See ref. 1, Table 1.

and 2.48 Å (X = I and Br, respectively), found for the pseudo-tetrahedral $[HgX_2(py)_2]$ molecules in the solid solvates correspond well with these peaks. The short distance, 2.4 Å, found for the $HgCl_2$ solution precludes the octahedral co-ordination found in the $HgCl_2(py)_2$ structure with bridging Hg–Cl distances around 2.7 Å, but is indicative of a pseudo-tetrahedral co-ordination.

The peak found at 1.4 Å for all three solutions is due to the N–C and C–C bond distances within the pyridine molecules and is satisfactorily explained by the calculated peak shapes [dotted lines in Figure 2(*b*)]. The diagonal distances at 2.4 and 2.7 Å in the pyridine rings are seen to make increasingly more important contributions to the peak in the Hg–X region for X = I, Br, and Cl. The concentration of pyridine is virtually the same in all three solutions (Table 1) and the size of the calculated pyridine peaks thus shows the relative magnitude of the other intramolecular contributions to the model functions in Figure 2.

The distinct peak observed at about 5.0 Å in the r.d.f. for the HgI_2 solution corresponds to the I···I distance of 5.052(2) Å in the $[HgI_2(py)_2]$ structure. The peak at 4.8 Å for the $HgBr_2$ solution is comparable to the Br···Br distance of 4.68 Å found in the $[HgBr_2(py)_2]$ structure. These values indicate that the molecular structure adopted in the crystalline state persists when the complexes are dissolved, and there is good agreement between the observed and calculated peak shapes for the Hg–X and X···X interactions within the bent HgX_2 moieties [solid lines (*i*) in Figure 2(*b*)].

As a consequence of the low scattering factor for Cl, the $HgCl_2$ solution shows no distinct peak for Cl···Cl interaction between 3.9 and 4.7 Å, a range which should encompass Cl···Cl distances likely in the tetrahedral and linear extremes. However, the intensity of the Hg–Cl peak is close to that predicted for two Hg–Cl bonds, although the fit is improved if the number of Hg–Cl interactions is reduced to 1.9. There are no grounds for invoking aggregated species as fragments of the structure adopted in the crystal. The best fit can be rationalized by introducing a small degree of Hg–Cl bond dissociation, an observation probably connected with the small amount of redistribution of the $HgCl_2$ species as indicated by the equilibrium constants for dilute solutions,[3] and by the above mentioned possible occurrence of minor species as revealed by our solution i.r. studies.

Up to 7 Å, there are several more or less diffuse peaks which can be related to the co-ordination of pyridine molecules. Peak shapes have been calculated based on a co-ordination model from the crystal structures. The pyridine ligands have been treated as entities with known geometry using the precise parameters given for the pyridine ligands in a crystal structure containing $ZnCl_xBr_{2-x}(py)_2$ complexes.[12] The intramolecular interactions involving pyridine have been divided into two categories.

The first, represented by the dashed lines in Figure 2(*b*), contain all Hg–N, C, and H distances. They can all be related directly to the Hg–N bond length, assuming no tilt angle of the pyridine molecule. The H atoms have been placed in calculated trigonal positions. The X···N and X···C(4) distances have also been included in this group. Especially at 3.5—4 and at 6 Å the corresponding peaks are distinguishable, but also in the X···X region around 5 Å there are substantial contributions. The Hg–N distances are not directly distinguishable for any of the solutions because of overlap with the Hg–X interactions, and the Hg–N parameters given in Table 5 are therefore evaluated mainly from the more resolved Hg–C interactions assuming a known pyridine geometry.

The second category consists of the remaining X···C distances which will vary with the twist angle around the Hg–N bond [solid lines (*ii*) in Figure 2(*b*)]. From molecular models, it is evident that the rotations of the pyridine groups would, to some extent, be hindered by interference between the rings at large twist angles. In the crystal structures, the twist angles of the pyridine ligands, from the symmetrical position with the pyridine plane perpendicular to the N,Hg,N plane, are rather small, 2.4 and 16.4° for $[HgBr_2(py)_2]$ and 27.7° for $[HgI_2(py)_2]$. Mean distances and root-mean-square variations, *l*, Table 5, have been estimated from calculations of distance variations from such restricted variations of the twist angle. Even though the contribution of this second category of distances is, especially for the $HgCl_2$ solution, more diffuse and smaller than from the first, the fit of the model function is considerably improved at about 4 and 6 Å. The parameter values and the shape of the peaks obtained by the fitting procedure indicate that the preferred conformation of the pyridine rings in solution on the average has small twist angles similar to those found in crystals.

Table 5. Final parameters[a] for the calculation of model functions for the $HgX_2(py)_2$ complexes in pyridine solution, with estimated standard deviations in parentheses for independently refined parameters

Parameter		X			$[HgI_2(py)_2]$	$[HgBr_2(py)_2]$
		I	Br	Cl		
Hg–X	*d*	2.665(2)	2.497(2)	2.375(10)	2.666	2.480
	l	0.070(3)	0.067(3)	0.071(6)		
	n	2.00(2)	1.96(3)	1.90(5)	2	2
X···X	*d*	5.02(2)	4.79(2)	4.59[b]	5.05	4.68
	l	0.14(2)	0.14(2)	0.14[b]		
	n	*n*(Hg–X)/2	*n*(Hg–X)/2	*n*(Hg–X)/2	1	1
Hg–N	*d*	2.43(2)	2.45(2)	2.47(2)	2.42_4	2.38_7
	l	0.12(2)	0.12(2)	0.12(2)		
	n	2	2	2	2	2
Hg···C(2), C(6)	*d*	3.317	3.336	3.355	3.32	3.26
	l	0.16	0.16	0.13		
	n	4	4	4	4	4
Hg···C(3), C(5)	*d*	4.647	4.667	4.686	4.65	4.61
	l	0.17	0.17	0.16		
	n	4	4	4	4	4
Hg···C(4)	*d*	5.168	5.197	5.217	5.16	5.14
	l	0.17	0.17	0.16		
	n	2	2	2	2	2
X···N	*d*	3.996	3.832	3.727	3.98	3.82
	l	0.14	0.14	0.14		
	n	4	4	4	4	4
X···C(4)	*d*	6.342	6.200	6.115	6.31	6.22
	l	0.20	0.20	0.17		
	n	4	4	4	4	4
X···C in pyridine ring (variable)[c]	*d*	4.02	3.872	3.790	4.06	3.90
	d	5.26	5.099	4.991	5.19	5.05
	d	5.32	5.187	5.115	5.35	5.22
	d	6.33	6.176	6.077	6.27	6.17
	l	0.20	0.20	0.17		
	n	4	4	4	4	4
Angle XHgX (°)[d]		141(2)	147(2)	150[b]	142.7(1)	141.2(1)

[a] *d* = Distance in Å, *l* = root-mean-square variation in the distance ($b = l^2/2$), and *n* = frequency of the distance relative to one mercury atom. The geometry of the pyridine ligand is fixed. A comparison with corresponding mean distances from the crystal structures of $[HgI_2(py)_2]$ and $[HgBr_2(py)_2]$ is given in the last two columns. [b] Estimated values. [c] Calculated for 0° twist angle, see text. [d] Without correction for shrinkage, see text.

The estimated standard deviations for the Hg–X and X···X interactions in Table 5 are obtained mainly from least-squares refinements of model intensities by minimizing the error square sum $U = \Sigma w(i_{calc.} - i_{exptl.})^2$ in a way described previously[4] for various lower limits of *s*. The basis for this refinement procedure is that the intensity contributions from well defined intramolecular interactions persist at high *s* values, while the diffuse intermolecular contributions fall off rapidly and often can be neglected in this range. No attempt was made to describe the liquid structure itself, *i.e.* the packing of the molecular species, in terms of an approximate model.

The result of such refinements has to be assessed with caution because of possible biases due to inadequacies or deficiencies in the model used, and deviations in parameter values due to *e.g.* correlations between overlapping distances or systematic errors in the data. An attempt to estimate the magnitude of such deviations was made by systematic variations of the model parameters held constant in a refinement. The effect on the refined main interactions has been taken into account in the parameter values and errors reported in Table 5. The fit obtained is shown in Figure 1, and is satisfactory for $s > 4$ Å^{-1}.

The sum of all peak shapes [dotted lines in Figure 2(*a*)] calculated for the $HgX_2(py)_2$ model with parameters according to Table 5 shows that two pyridine molecules co-ordinated to HgX_2 explain all main peaks of the experimental curves. The differences between the r.d.f.s and the model functions (dashed lines) are similar for all three solutions. No prominent features remain except for a broad peak around 6 Å which is due to intermolecular atomic distances in the solution.

The vibrational movements of the halide atoms perpendicular to the Hg–X bonds will cause the observed X···X distance to be shorter than its equilibrium value; the so-called Bastiansen–Morino shrinkage effect.[13] For a linear HgI_2 molecule in the gas phase this apparent shortening of the I···I distance, compared to twice the Hg–I distance, has been calculated from vibration frequencies to be 0.044 Å, 0.039 Å for $HgBr_2$,[13] and 0.036 Å for $HgCl_2$.[14] In the present slightly bent structures the effect would be smaller for the same amplitudes, but this is counteracted because of the larger vibrational amplitudes [*l* values obtained for I···I are 0.069 Å in the gas phase,[13] 0.10(1) Å in dmso,[4] and 0.14(2) Å in pyridine]. The shrinkage can therefore be roughly estimated to be of the same magnitude as in the gas phase. The corrected XHgX angles would then be 143 and 151° for X = I and Br, respectively, including the shrinkage calculated for linear gas-phase molecules. Although this correction is based on rather qualitative estimates, the precision of the present data does not seem to merit a more elaborate calculation.

For the $HgCl_2$ solution, where the contributions to the r.d.f. from the co-ordinated pyridine ligands are the most prominent, the contribution from expected interactions between the two pyridine rings has been calculated [dotted line (*iii*) in Figure 2(*b*)]. The NHgN angle was assumed to be about 90°. A slight improvement of the fit resulted, but this additional contribution

is minor and diffuse and can safely be neglected for the other solutions.

Discussion

Mercury(II) displays great diversity in its stereochemistry. Donors which seek a high *s*-orbital content in bonding are apt to limit the tendency of mercury to expand its co-ordination number above two, the most extreme case being found in $HgMe_2$. Even when four-co-ordination is achieved, there are large deviations from tetrahedral angles within the co-ordination sphere. This is illustrated by the structural parameters of a set of $[HgX_2(PPh_3)_2]$ complexes (Table 6). The PHgP angles range from 94.8° (X = CF_3)[14] to 134.1° (X = Cl)[15] with the XHgX angles being 146.6 and 110.7°, respectively. The smaller PHgP angles tend to be associated with the longer Hg–P bond lengths and lower *s*-orbital content of the hybrid orbital used by mercury in its bonding with phosphorus.

On a similar basis, the increase in Hg–N bond lengths of $[HgX_2(py)_2]$ complexes in solution from X = I to X = Cl might be expected to be accompanied by an increase in XHgX angles. This is clearly the case between X = I and X = Br (Table 7). That the XHgX angles are considerably greater than the tetrahedral value is a clear indication that halide is a better donor towards Hg^{II} than is pyridine. However, this analogy would also imply that the tendency towards wider XHgX angles in the sequence from X = I to X = Cl corresponds to an increasing *s*-orbital content in the Hg–X bond, although the softness of the halide atom decreases. It might also have been anticipated that the Hg–N bond length in solution would correlate with the heats of solvation of gaseous HgX_2 in pyridine, but the opposite trend is found (Table 7). Factors other than Hg–N bond formation are clearly involved. The most important of these is likely to be the association between pyridine and the residual charge on the bound halide which should be highest for the chloride.[16] Already for the free halide ions with the same integral charge, the solvation enthalpies in pyridine and other donor solvents are strongly correlated with the charge/radius ratio and are thus highest for the chloride.[17]

These observations lead to the conclusion that the decreasing solvation of the mercury atom is outweighed by the increasing interaction between the solvent molecules and the halide atoms in HgX_2 in the sequence I to Cl. This electron donation from the halide atoms to the solvent is likely to reduce the electrostatic contribution to the Hg–X bond. A compensating increase in *s*-orbital participation from the mercury atom would then be consistent with the observed increase in XHgX angles and Hg–N bond length. A similar trend of increasing XHgX angles and increasing heats of solvation is also found for dmso solutions of HgX_2 (Table 7).

An interesting comparison can be made with the crystal structures of the $HgX_2(py)_2$ compounds, where no excess of solvent can influence the molecular structure. In the molecular structures of $[HgI_2(py)_2]$ and $[HgBr_2(py)_2]$ the halide atoms are surrounded by pyridine ligands from neighbouring molecules in a similar way, although the interactions are restricted by

Table 6. Average bond lengths and interbond angles in some crystalline monomeric $[HgX_2(PPh_3)_2]$ complexes

	Bond lengths (Å)		Bond angles (°)	
X	HgP	HgX	P–Hg–P	X–Hg–X
CF_3[a]	2.91(2)	2.12(2)	94.8(1)	146.6(9)
CN[b]	2.515(7)	2.234(26)	108.9(2)	108.5(15)
I[c]	2.566(3)	2.748(1)	109.0(1)	110.4(1)
Br[d]	2.538(16)	2.630(8)	113.0(5)	106.9(3)
SCN[e]	2.488(3)	2.571(3)	118.1(1)	96.7(1)
ONO_2[b]	2.451(1)	2.507(4)	131.8(1)	70.0(2)
Cl[d]	2.470(2)	2.552(3)	134.1(1)	110.7(1)

[a] Ref. 14. [b] H. B. Buergi, R. W. Kunz, and P. S. Pregosin, *Inorg. Chem.*, 1980, **19**, 3707. [c] L. Fälth, *Chem. Scr.*, 1976, **9**, 71. [d] Ref. 15. [e] R. C. Makhija, A. L. Beauchamp, and R. Rivest, *J. Chem. Soc., Dalton Trans.*, 1973, 2447.

Table 7. Comparison of symmetric (ν_1) and asymmetric (ν_3) vibration stretching frequencies, Hg–X bond distances, X–Hg–X angles, and solvation enthalpies for the mercury dihalides in the gas phase and in solution

$\nu_1,\nu_3/cm^{-1}$	Gas	Methanol	dmso	Pyridine	$HgX_2(PEt_3)_2$ solid[a]
$HgCl_2$	358,[b] 413[c]	322,[d] 369[e]	303,[d] 341[e]	282,[f] 313[e]	189, 176
$HgBr_2$	222,[b] 293[c]	208,[f] 262[e]	195,[d] 241[e]	183,[f] 222[e]	152, 132
HgI_2	158,[b] 237[g]	151[f]	145,[d] 193.4[e]	142,[f] 181[e]	110, 109
d(Hg–X)/Å					
$HgCl_2$	2.25[h]	2.308(3)[d]	2.32,[i] 2.35[d]	2.375(10)	2.68(1)
$HgBr_2$	2.41[j]		2.455(3)[d]	2.497(2)	
HgI_2	2.554(3)[k]		2.625(2)[d]	2.665(2)	
X–Hg–X/°					
$HgCl_2$	180 ± 16[h]	*ca.* 170[d]	*ca.* 165[d]		105.5(5)
$HgBr_2$	180 ± 20[j]		165(3)[d]	151(3)	
HgI_2	180 ± 10[j]		159(2)[d]	143(2)	
$-\Delta H_{sv}°$/kJ mol^{-1}					
$HgCl_2$		84[i]	104[l]	138[i]	
$HgBr_2$		81[i]	101[l]	136[i]	
HgI_2		76[i]	93[l]	130[i]	

[a] N. A. Bell, T. D. Dee, P. L. Goggin, M. Goldstein, R. J. Goodfellow, T. Jones, K. Kessler, D. M. McEwan, and I. W. Nowell, *J. Chem. Res.*, 1981, (*S*) 2, (*M*) 0201. [b] Raman value (R. J. H. Clark and D. M. Rippon, *J. Chem. Soc., Faraday Trans. 2*, 1973, 1496). [c] I.r. value (W. Klemperer and L. Lindeman, *J. Chem. Phys.*, 1956, **25**, 397). [d] Raman or *X*-ray diffraction value.[4] [e] I.r. value, this work. [f] Raman value, this work. [g] I.r. value (W. Klemperer, *J. Chem. Phys.*, 1956, **25**, 1066). [h] K. Kashiwabara, S. Konaka, and M. Kimura, *Bull. Chem. Soc. Jpn.*, 1973, **46**, 410. [i] I. Persson, unpublished work. [j] P. A. Akiskin, V. P. Spiridonov, and A. N. Khodchenkov, *Zh. Fiz. Khim.*, 1959, **33**, 20. [k] V. P. Spiridonov, A. G. Gershikov, and B. S. Butayev, *J. Mol. Struct.*, 1979, **52**, 53. [l] S. Ahrland, L. Kullberg, and R. Portanova, *Acta Chem. Scand., Ser. A*, 1978, **32**, 251; the values have been recalculated using the critically appraised lattice enthalpies $\Delta H_f°$ (L. G. Hepler and G. Olafsson, *Chem. Rev.*, 1975, **75**, 585).

the packing restraints of the crystal. The geometry of the $[HgI_2(py)_2]$ molecule, which even in solution has weak solvation of the iodine atoms, is virtually unaffected by a change *in environment* (Table 5). In the solid $[HgBr_2(py)_2]$ solvate, however, the weaker Br • • • py interactions than in solution are consistent with the smaller BrHgBr angle (even smaller than IHgI) and the shorter Hg–N bond. The hampering in the solids of the stabilizing X • • • py interactions should be most pronounced in the chloride complex. This is likely to be an important factor influencing the preference of $HgCl_2(py)_2$ for the chain-type structure, where the chlorine atoms form bridges between the mercury atoms.

A number of properties of $[HgX_2L_2]$ complexes are compared in Table 7. Complex formation lowers the HgX_2 stretching frequencies to an extent which depends on the donor. The effect on the wavenumber of the asymmetric mode is greater than that for the symmetric mode, and when the donor is a trialkylphosphine the former is actually the lower. For chlorides there is a remarkably good correlation between either of these frequencies and Hg–Cl bond lengths, especially since such a comparison is taking no account of kinetic, interaction, or vibrational mixing effects which must vary considerably between these complexes.

Acknowledgements

We thank the Swedish Natural Science Research Council, the Knut & Alice Wallenberg Foundation, the S.E.R.C. (U.K.) and the S.R.C. (U.K.) for financial support and for grants towards equipment.

References

1 R. M. Barr, M. Goldstein, and W. D. Unsworth, *J. Cryst. Mol. Struct.*, 1974, **4**, 165.
2 A. J. Canty, C. L. Raston, B. W. Skelton, and A. H. White, *J. Chem. Soc., Dalton Trans.*, 1982, 15 and refs. therein.
3 S. Arhland, S. Ishiguro, A. Marton, and I. Persson, *Acta Chem. Scand., Ser. A*, in the press.
4 M. Sandström, *Acta Chem. Scand., Ser. A*, 1978, **32**, 627; F. Gaizer and G. Johansson, *ibid.*, 1968, **22**, 3013.
5 G. Johansson, *Acta Chem. Scand.*, 1971, **25**, 2787; *ibid.*, 1966, **20**, 553.
6 G. Johansson and M. Sandström, *Chem. Scr.*, 1973, **4**, 195.
7 M. Sandström, I. Persson, and S. Ahrland, *Acta Chem. Scand., Ser. A*, 1978, **32**, 607.
8 'International Tables for *X*-Ray Crystallography,' Kynoch Press, Birmingham, 1974, vol. 4.
9 G. Kopfmann and R. Huber, *Acta Crystallogr., Ser. A*, 1968, **24**, 348; A. C. T. North, D. C. Phillips, and F. Scott Mathews, *ibid.*, p. 351.
10 G. M. Sheldrick, SHELX 76, Program for crystal structure determination, University of Cambridge, 1976.
11 D. N. Waters and Z. Kantarci, *J. Raman Spectrosc.*, 1977, **6**, 251 and refs. therein.
12 B. E. Villarreal and E. O. Schlemper, *J. Cryst. Mol. Struct.*, 1978, **8**, 217.
13 S. J. Cyvin, 'Molecular Vibrations and Mean Square Amplitudes,' Elsevier, Amsterdam, 1968, p. 311.
14 D. J. Brauer, Abstracts IXth International Conference on Organometallic Chemistry, Dijon, 1979, B59.
15 N. A. Bell, T. D. Doe, M. Goldstein, P. J. McKenna, and J. W. Nowell, *Inorg. Chim. Acta*, 1983, **71**, 135.
16 L. Dixit, *Appl. Spectrosc. Rev.*, 1984, **20**, 159 and refs. therein.
17 A. Ahrland, *Pure Appl. Chem.*, 1982, **54**, 1451.

Received 22*nd October* 1984; *Paper* 4/1800